JCTC Journal of Chemical Theory and Computation

pubs.acs.org/JCTC Article

Active Learning of the Conformational Ensemble of Proteins Using Maximum Entropy VAMPNets

Diego E. Kleiman and Diwakar Shukla*

Cite This: https://doi.org/10.1021/acs.jctc.3c00040 Read Online

ACCESS | Metrics & More | Article Recommendations | Supporting Information

ABSTRACT: Rapid computational exploration of the free energy landscape of biological molecules remains an active area of research due to the difficulty of sampling rare state transitions in molecular dynamics (MD) simulations. In recent years, an increasing number of studies have exploited machine learning (ML) models to enhance and analyze MD simulations. Notably, unsupervised models that extract kinetic information from a set of parallel trajectories have been proposed including the variational approach for Markov processes (VAMP), VAMPNets, and time-lagged variational autoencoders (TVAE). In this work, we propose a combination of adaptive sampling with active learning of kinetic models to accelerate the discovery of the conformational landscape of biomolecules. In particular, we introduce and compare several techniques that combine kinetic models with two adaptive sampling regimes (least counts and multiagent reinforcement learning-based adaptive sampling) to enhance the exploration of conformational ensembles without introducing biasing forces. Moreover, inspired by the active learning approach of uncertainty-based sampling, we also present MaxEnt VAMPNet. This technique consists of restarting simulations from the microstates that maximize the Shannon entropy of a VAMPNet trained to perform the soft discretization of metastable states. By running simulations on two test systems, the WLALL pentapeptide and the villin headpiece subdomain, we empirically demonstrate that MaxEnt VAMPNet results in faster exploration of conformational landscapes compared with the baseline and other proposed methods.

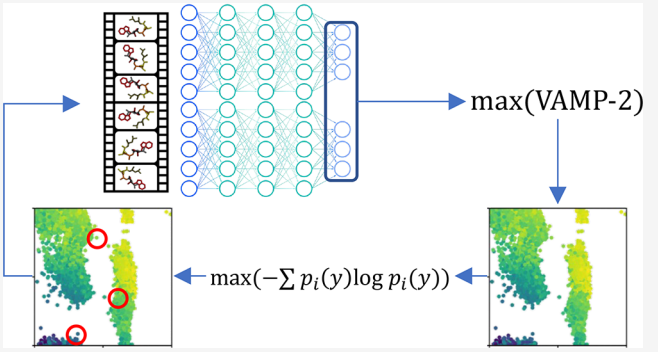

1. INTRODUCTION

Molecular dynamics (MD) simulations have become a widely applied computational tool to disentangle the details of nanoscopic systems relevant to a wide range of fields, from materials engineering[1,2] to fundamental biology.[3] The reason for their widespread use lies in their ability to resolve the dynamics of molecular systems at excellent time and space resolutions. Nonetheless, the fine-grained time steps of MD simulations also result in high computational costs if the processes to be observed occur at long time scales. Precisely, the time interval at which an MD simulation can update atomic positions is typically restricted to the order of femtoseconds, whereas most molecular processes of interest take place at the microsecond to millisecond scale. In biology, examples of such processes include transport across transmembrane proteins,[4,5] signal relays,[6,7] ligand binding,[8,9] and protein folding.[10]

A myriad of approaches have emerged to tackle the long time scale challenge in atomistic MD simulations.[11] While numerous methods enhance the sampling of the system by modifying the potential function or the thermodynamic ensemble,[12−14] others pursue the same goal by selectively restarting trajectories from initial conditions that favor a sampling criterion[15−17] (see the Adaptive Seeding section in ref 11). Different problems have been studied by using both types of methods, sometimes in combination, with satisfactory results.[18,19] The choice of a suitable method will largely depend on the nature of the problem at hand. In general, adaptive seeding methods are well-suited to exploit the capabilities of large computer clusters through massively parallel simulations[20,21] and to recover the unbiased kinetics of the system through statistical models such as Markov state models (MSMs).[22]

For biological systems, the thermodynamic ensembles of interest are typically isothermal−isobaric ensembles. Consequently, the probability of sampling a state decays with its energy following a Boltzmann distribution. For this reason, one of the challenges associated with the long time scale problem in MD simulations is the sampling of rare or transition states, which are characterized by high energies and low probabilities. While biased methods can accelerate the sampling of rare

Special Issue: Machine Learning for Molecular Simulation

Received: January 9, 2023

states, this advantage may come at the cost of sampling an unphysical transition. In this work, we investigate the ability of unbiased simulations to explore a diverse conformational ensemble, and therefore, our proposed techniques fall under the adaptive seeding category.

Adaptive seeding methods can be divided into weighted ensemble and adaptive sampling techniques.[11] Weighted ensemble techniques rely on the "splitting" and "merging" of trajectories according to their relative importance for a sampling criterion. In these methods, weights for each trajectory are tallied; splitting reduces the weight, and merging increases it. These weights are introduced with the goal of recovering statistically unbiased observables.[23] On the other hand, adaptive sampling techniques tend to prioritize the exploration of a diverse set of molecular conformations by iteratively restarting short simulations from poorly sampled states. In past approaches, these states are obtained by using some discretization of the conformational space, such as clustering. After satisfactory coverage of the conformational landscape is obtained, the short trajectories are statistically unbiased using, for instance, MSMs.[24] All methods presented in this study fall within the adaptive sampling category.

Machine learning (ML) is becoming critically relevant to the field of enhanced MD simulations. In particular, ML techniques have been utilized to model force fields,[25−27] approximate optimal biasing potentials,[28,29] derive reaction coordinates,[30,31] and extract information from MD data.[32] For adaptive sampling, in particular, manifold learning[33,34] and reinforcement learning (RL) algorithms[17,33,35,36] have been applied in the past to guide simulations. Among ML methodologies, deep neural networks (DNNs) are especially promising because of their ability to learn arbitrarily complex nonlinear functions.[37]

An interesting application of ML models to MD that motivates the current study is the extraction of kinetic information from a set of trajectories. The reason is that kinetics can potentially be exploited to improve the selection of initial conditions for adaptive sampling. The variational approach to Markov processes (VAMP)[38,39] can discover an optimal mapping from input features (functions of the degrees of freedom of the system) and the slow reaction coordinates of the process. This is achieved by maximizing a variational score, often termed the VAMP score.[39] A family of DNN models that are trained to maximize the VAMP score for a set of trajectories has also been proposed,[40,41] with the simplest of them being termed VAMPNet.[40] In contrast to the linear approach used in VAMP (see feature TCCA),[39] the DNN models can find nonlinear combinations of features and may incorporate soft state discretization as part of their architecture.[40]

A priori, it is unclear how to use the output of a DNN model that maximizes a VAMP score to guide adaptive sampling simulations. When such a model is fitted without a discretization layer, the mapping can be interpreted as a learned embedding spanned by the slowest-changing collective variables (CVs) or reaction coordinates (RCs) of the system. This is a dimensional reduction if the output layer is smaller than the input layer. In this case, one may employ the DNN model in a similar way VAMP[38,39] or time-lagged independent component analysis (tICA)[42−44] are used in adaptive sampling workflows: the model projects the conformations along the slow processes and the state discretization and selection take place in this learned embedding. This is expected to improve performance when it is difficult to resolve state transitions in feature space, and the number of dimensions must be reduced to achieve a reasonable clustering.

When incorporating the state discretization layer (usually realized as a softmax operation[40]), the output of these models can be interpreted as the membership probabilities of a microstate in the kinetically metastable states. Given this probabilistic interpretation, we propose incorporating an information theoretic metric to guide the choice of new restarting points for adaptive sampling. Shannon entropy is a metric that reveals the uncertainty of a model against the possible outcomes of an event (in this case, the uncertainty of the model in placing a microstate into a metastable state). It has been connected to statistical mechanics[45] and used to combine experimental data with MD simulations.[46−48] A popular adaptive sampling technique, Least Counts, may be cast as a maximum entropy method, where the entropy is taken over the sampled state space, although there is no explicit usage of Shannon's metric. In this study, we empirically show that selecting the microstates that maximize the Shannon entropy of a VAMPNet leads to improved exploration in adaptive sampling, measured as the volume of CV or tIC space observed by the generated trajectories. We term this method maximum entropy (MaxEnt) VAMPNet. The workflow is as follows: after collecting some initial MD trajectories, a VAMPNet is fit to the data. Then, the VAMPNet is used to calculate state-assignment probabilities for all conformations. A limited number of conformations that obtain the highest entropy values are used as seeds for the following round of simulations. The process is iterated after retraining the VAMPNet with the new data. Sampling is terminated once exploration of the landscape is satisfactory.

Recent work by Tian et al.[49] also exploits the idea of retraining an ML model (in this case, a variational autoencoder or VAE) in successive rounds of adaptive sampling simulations. The current study differs from that work in two main aspects: (1) we use time-lagged ML models to learn kinetically relevant latent spaces (as opposed to learning a latent representation of structure space) and (2) MaxEnt VAMPNet uses the entropy to select new simulation seeds (as opposed to the lowest probability structures).

We divide our study in two phases: in the initial exploratory phase, we focused on three kinetic models available in the Python library deeptime,[50] VAMP,[39] VAMPNets,[40] and time-lagged variational autoencoders (TVAEs),[41] and combined them with two adaptive sampling methods: least counts (LC) adaptive sampling and multiagent reinforcement-learning-based adaptive sampling (MA REAP).[17] LC is a common baseline for adaptive sampling; in this technique, the states are obtained by clustering, and the starting structures are selected from the clusters with the fewest members.[51] In MA REAP, the states are also obtained by clustering, but the starting structures are selected by following a reward function that depends on the deviation of the structure with respect to the mean of the data.[17] We compared these methods based on their ability to explore the conformational landscape of a flexible pentapeptide (sequence WLALL).[52] Inspired by the results from these comparisons, we introduced the entropic metric for VAMPNets in the second phase of the study, where we showed that this last method achieves superior exploration when applied to two systems of different complexity: the WLALL pentapeptide and a fast-folding protein subdomain, the villin headpiece.[53]

https://doi.org/10.1021/acs.jctc.3c00040
J. Chem. Theory Comput. XXXX, XXX, XXX−XXX

The rest of the paper is organized as follows: the section explains all of the techniques introduced and compared in this paper. The section is divided into three parts. In the first part, we present the results of the exploratory phase of the study. In the second part, we introduce the Shannon entropy criterion with VAMPNets for adaptive sampling and compare it with the techniques analyzed in the exploratory phase. Lastly, we compare the two most promising methods in a realistic system (the villin headpiece protein) to validate the results observed in the previous subsection. We conclude with a discussion of the advantages and limitations of our proposed methods.

2. METHODS

2.1. Coupling Adaptive Sampling and Active Learning. Adaptive sampling MD is an iterative technique in which the conformational landscape of a molecular system is progressively discovered by restarting simulations from poorly sampled states. Typically, the iteration is divided into two steps: running trajectories and data analysis. In the first step, trajectories are initiated from the specified conformations. In the second step, the sampled points are clustered to discretize the conformational landscape into distinct states. Subsequently, a strategy is employed to determine which states to initiate the simulations anew. In the next iteration, new trajectories are executed from the selected states. This process continues until the sampling is satisfactory. The selection strategy for the restarting points has a profound impact on the sampling behavior.[15,54] Since only unbiased trajectories are typically utilized during adaptive sampling, the restarting selection strategy is the hinge point that researchers manipulate to alter the behavior of their algorithms.

Interestingly, there is a subset of ML termed active learning[55] that realizes training as an iterative process where a model is first fit to an available data set, and then new data points are queried to an oracle based on some criterion that maximally improves learning. Active learning has previously been used in combination with MD simulations to efficiently explore chemical space[56−58] and to find model parameters.[59] Since both adaptive sampling and active learning follow a two-stage process, we can couple both techniques. In other words, the data analysis phase of adaptive sampling becomes the learning phase of active learning. Similarly, the MD integrator acts as the oracle, so the querying phase of active learning becomes the simulation step in adaptive sampling. The information extracted by the ML model is used to select the restarting points for new simulations, which, in turn, will be utilized to refine the model in the next iteration. This workflow is summarized in Algorithm 1.

Algorithm 1 Coupled active learning–adaptive sampling

Input: potential $V(\boldsymbol{x})$, machine learning model $\mathcal{Y}$, reward/acquisition function $\mathcal{R}$, number of epochs E, trajectory length T, trajectories per epoch M

Sample initial data X^0 starting from $V(\boldsymbol{x}_0)$
for e in $1 \dots E$ **do**
  Train $\mathcal{Y}$ on X^{e-1}
  $Y^{e-1} = \mathcal{Y}(X^{e-1}) = [\mathcal{Y}(\boldsymbol{x}_0) \dots \mathcal{Y}(\boldsymbol{x}_{eTM})] = [\boldsymbol{y}_0 \dots \boldsymbol{y}_{eTM}]$
  $\boldsymbol{r} = \mathcal{R}(Y^{e-1}) = [\mathcal{R}(\boldsymbol{y}_0) \dots \mathcal{R}(\boldsymbol{y}_{eTM})]$
  Let $X_M = \{\boldsymbol{x}_m\}$ such that $\{\mathcal{R}(\mathcal{Y}(\boldsymbol{x}_m))\}$ achieves the max-M-sum in $\boldsymbol{r}$
  for all $\boldsymbol{x}_m \in X_M$ **do**
    Sample T new data starting from $V(\boldsymbol{x}_m)$
  end for
  Concatenate new data to X^{e-1} to obtain X^e
end for

In Algorithm 1, the function $\mathcal{R}$ outputs a scalar that is used to rank the conformations according to how desirable it is to restart simulations from them. Depending on the adaptive sampling regime employed, an additional model might be used to optimize $\mathcal{R}$.[17,60] For this reason, $\mathcal{R}$ can be interpreted as a reward function when the adaptive sampling regime depends on a RL model or an acquisition function when it does not.

2.2. Combining Kinetic Models with Adaptive Sampling Regimes. For Algorithm 1 to work, we must identify a suitable model $\mathcal{Y}$ that is able to extract useful information from the parallel trajectories. A relevant family of models[39−41,44] is based on identifying the slowest processes that occur in a system. Arguably, these processes will be rate-limiting for state transitions. The models learn the slowest processes by finding the transformations that maximize a variational score for a set of trajectories, which is usually termed the VAMP score.[39] In mathematical terms, for a set of trajectories $\{X^i\}_{i=1}^N$ where $X^i = [\boldsymbol{x}_0^i \dots \boldsymbol{x}_T^i]$, we can compute the covariance matrices C_{00} and C_{11}, and time-lagged covariance matrix C_{01} as follows[39,40]

$$C_{pq} \approx \frac{1}{N}\sum_{i}^{N} \frac{1}{T-\tau} \sum_{t=1+q\tau}^{T-p\tau} \chi_p(\boldsymbol{x}_t^i)\chi_q(\boldsymbol{x}_{t+(q-p)\tau}^i)^{\mathrm{T}} \tag{1}$$

where p and q must be replaced by 0 or 1 and τ is the lag time measured in time steps. χ_0 and χ_1 represent transformations from features or CVs to latent variables. It is possible to have χ_0 and χ_1 be identical, and these transformations can be machine-learned through stochastic methods.[40] Once these matrices have been estimated from data, they are preprocessed to remove the mean and obtain centered covariance matrices $\overline{C}_{00}$, $\overline{C}_{01}$, and $\overline{C}_{11}$. Then a version of the VAMP score (VAMP-2)[39] can be computed as

$$\hat{R}_2 = \left\| \overline{C}_{00}^{-\frac{1}{2}} \overline{C}_{01} \overline{C}_{11}^{-\frac{1}{2}} \right\|_F^2 + 1 \tag{2}$$

where the norm F is the Frobenius norm.

Different ML models have been proposed to find the transformations $\{\chi_0, \chi_1\}$ and have been implemented in deeptime.[50] Namely, the models that we employ in this

https://doi.org/10.1021/acs.jctc.3c00040
J. Chem. Theory Comput. XXXX, XXX, XXX−XXX

study are VAMP,[39] VAMPNets,[40] and TVAEs.[41] By using the VAMP-2 score as the gain function, these models learn useful mappings from the input features to the slowest-changing processes in the system.[39−41] These learned embeddings can be used to discriminate between kinetically different states. If the output of the model has fewer dimensions than the input feature vector, then the model performs a dimensionality reduction.

In this study, we use VAMP to refer to feature time-lagged canonical correlation analysis (feature TCCA).[39] Time-lagged independent component analysis (tICA)[42,43] and the variational approach to conformational dynamics (VAC)[38] are subclasses of this technique. In this case, the basis sets $\{\chi_0, \chi_1\}$ are simply the user-defined features or CVs. VAMP works by performing a truncated singular value decomposition on the matrix $C_{00}^{-1/2}C_{01}C_{11}^{-1/2}$ to obtain $U'KV'^{\mathrm{T}}$. Then the coefficient matrices U and V are computed as $U = C_{00}^{-1/2}U'$ and $V = C_{11}^{-1/2}V'$. Finally, the learned projections, i.e., the left and right singular functions, can be found as $\mathbf{u}_i^{\mathrm{T}}\chi_0$ and $\mathbf{v}_i^{\mathrm{T}}\chi_1$ respectively, where $\boldsymbol{u}_i$ and $\boldsymbol{v}_i$ are the ith column vectors of U and V.[39,50]

In contrast to VAMP, VAMPNets are based on DNNs. They are typically implemented as multilayer perceptrons (MLPs), but other architectures have been proposed.[61] Although in their original form VAMPNets were designed with a softmax layer for output processing to learn a soft discretization, they can also be utilized without one to learn the projection from feature space onto the slow variables of the system. There exists literature that refers to such models as "state-free" VAMPNets.[62] The transformations $\{\chi_0, \chi_1\}$ can be stochastically learned by DNNs because the variational score in eq 2 is differentiable, and thus the update gradient is well-defined.[40]

TVAEs can be conceived as extensions of VAMPNets where the DNN employed is a variational autoencoder. This is a network that consists of an encoder, which compresses the input at time t into a small number of dimensions or a latent space. Then, the decoder reconstructs the input from the compressed dimensions at time $t + \tau$. Since this is a time-lagged autoencoder, the encoder essentially performs a nonlinear version of TCCA.[50] The variational qualifier refers to the fact that the TVAE learns a probability distribution over the latent space as opposed to simply mapping inputs to fixed points on the dimensionally reduced coordinates. The use of variational autoencoders offers the possibility of employing the trained model for generative tasks.[50] However, as presented in the Results and Discussion, the TVAE-based sampling techniques did not perform on par with the VAMPNet-based ones.

In the exploratory phase of this study, we asked whether combining such kinetic models with different adaptive sampling schemes would yield better exploration performance. We tested two adaptive sampling schemes: least counts (LC) and multiagent reinforcement learning-based (MA REAP) adaptive sampling. While the former is a typical baseline for adaptive sampling, the latter utilizes a more complex reward function to select the restarting points for simulation.

When employing LC adaptive sampling in combination with a kinetic model, we project the conformations onto the learned embedding and then cluster the data points into discrete states. To seed the next round of simulations, we choose the centers of those clusters with the fewest number of members. In other words, $\mathcal{R}$ is the inverse of the frame count that falls in the same cluster as the evaluated conformation.

To combine these kinetic models with MA REAP, the first steps are identical as for LC: project the conformations, cluster them, select cluster centers as the states, and select a subset of candidates on the basis of the least counts criterion. However, when employing MA REAP, the starting structures are selected through a stakes-based reward function[17]

$$\mathcal{R}(\boldsymbol{y}, \{\boldsymbol{\mu}_t^a\}_{a=1}^N, \{\boldsymbol{\sigma}_t^a\}_{a=1}^N, \{\mathbf{w}_t^a\}_{a=1}^N) = \sum_a^N s_{\boldsymbol{y}}^a \sum_i^K w_{i,t}^a \frac{|y_i - \mu_{i,t}^a|}{\sigma_{i,t}^a} \tag{3}$$

where N is the number of agents and K is the number of output dimensions. $\boldsymbol{y}$ is a cluster center or state (projected onto the embedding learned by $\mathcal{Y}$), and $\boldsymbol{\mu}_t^a$ and $\boldsymbol{\sigma}_t^a$ are the mean and standard deviation of the data (as estimated up to time t) for agent a. $s_{\boldsymbol{y}}^a$ represents the stake that agent a has on state $\boldsymbol{y}$, which becomes relevant only when multiple agents are scouting the conformational landscape. The stake essentially determines which agent collects the data from a trajectory started at $\boldsymbol{y}$ to change its estimates of $\boldsymbol{\mu}_t^a$ and $\boldsymbol{\sigma}_t^a$. $w_{i,t}^a$ represents the weight that is assigned to a given dimension; therefore, if a conformation displays a larger deviation along a latent variable with a higher weight, the reward is larger. The inner sum of eq 3 can be interpreted as a weighted standardized Euclidean distance. Both $s_{\boldsymbol{y}}^a$ and $\boldsymbol{w}_t^a$ are fit from the trajectories, but $s_{\boldsymbol{y}}^a$ is determined at the clustering step and $\boldsymbol{w}_t^a$ is set to maximize $\mathcal{R}$ through quadratic optimization.[17,60]

One may ask if, in the multiagent case, one distinct version of $\mathcal{Y}$ should be learned by each agent given only their own data. If this were the case, the outer sum in eq 3 would lack a meaningful interpretation, since the K output dimensions would differ across agents. Therefore, we restrict all agents to use the same instance of a kinetic model. It might be possible to modify eq 3 to accommodate the alternative design choice, but this is outside the scope of the present study. Learning different versions of $\mathcal{Y}$ may alter the behavior of the algorithm by forcing agents to rely on local kinetic maps, rather than on a global model.

Utilizing the three aforementioned kinetic models with two adaptive sampling regimes yields six combinations, which are denominated {VAMP, VAMPNet, TVAE} + {LC, MA REAP} according to the model and the regime employed in each case.

2.3. Maximum Entropy VAMPNets. Unlike the previously described approaches, where the model $\mathcal{Y}$ projects a conformation onto the slow-changing dimensions of the system, here we are interested in VAMPNets that perform a "fuzzy clustering" by incorporating a final softmax layer. The softmax operation can be expressed as

$$p_i(\boldsymbol{y}) = \frac{e^{y_i}}{\sum_k^K e^{y_k}} \tag{4}$$

where $p_i(\boldsymbol{y})$ can be interpreted as the probability that conformation $\boldsymbol{y}$ is in the output state $i \in \{1, ..., K\}$. For VAMPNet, each output state corresponds to a kinetically distinct state or metastable state. Due to this probabilistic interpretation, we can compute the Shannon entropy for a given conformation:

$$H(\boldsymbol{y}) = -\sum_i^K p_i(\boldsymbol{y}) \log p_i(\boldsymbol{y}) \tag{5}$$

https://doi.org/10.1021/acs.jctc.3c00040
J. Chem. Theory Comput. XXXX, XXX, XXX−XXX

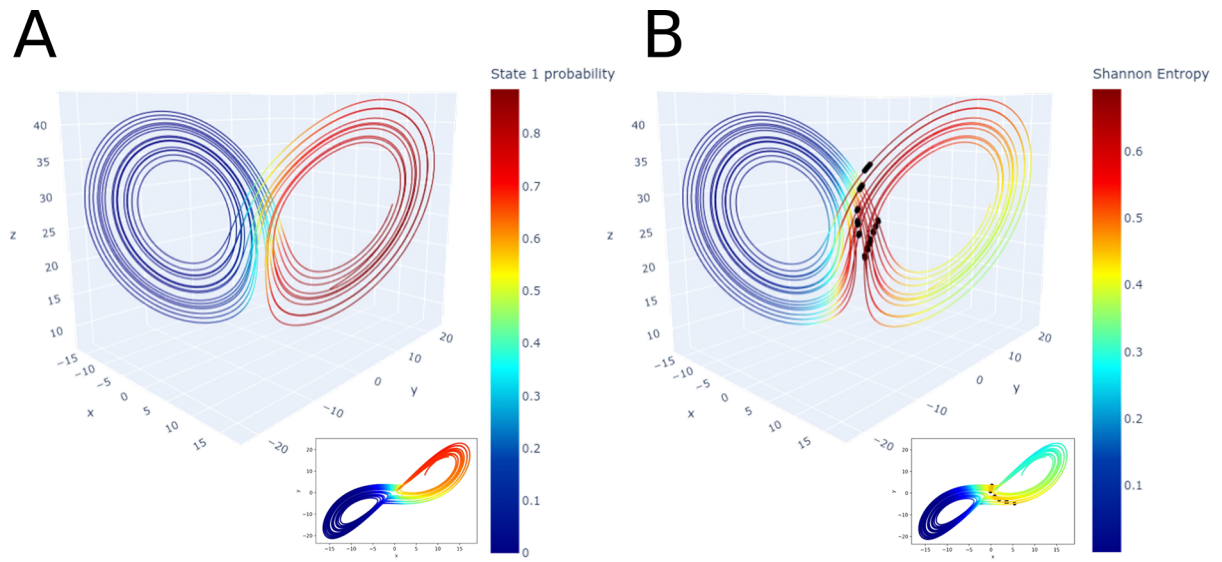

Figure 1. Illustration of the MaxEnt VAMPNet selection criterion in the original Lorenz system.[63] (A) Projection of state 1 probabilities on the validation trajectory. Inset shows projections on the $x-y$ plane. (B) Projection of the Shannon entropy on the validation trajectory. Black dots indicate the 20 data points with the highest entropy. Inset shows projection on the $x-y$ plane. It can be observed that the entropy maxima occur at the interface between states.

which is maximized when the predicted probability over the K output states is uniform or $p_i(\boldsymbol{y}) = 1/K\ \forall i$. In other words, $H(\boldsymbol{y})$ is maximized when the model is uncertain to which metastable state the conformation "belongs". H can be interpreted as a choice for $\mathcal{R}$ in Algorithm 1 when the output of $\mathcal{Y}$ is a probability distribution.

In the active learning community, the Shannon entropy is one of the most general and popular choices of uncertainty metric.[55] Nonetheless, to the best of our knowledge, uncertainty sampling has never been used in combination with VAMPNets, including entropy-based sampling. In our proposed adaptive sampling technique, after $\mathcal{Y}$ has been fit to the data and the membership probabilities $p_i(\boldsymbol{y})$ have been obtained, the Shannon entropy, $H(\boldsymbol{y})$, of each conformation (or a representative subset when memory becomes a concern) is computed. Then, the structures that maximize $H(\boldsymbol{y})$ are selected to seed the next round of simulations, and the workflow of Algorithm 1 proceeds. The intuition behind this method is that the VAMPNet will select structures that cannot be easily categorized, and therefore the conformations that are poorly sampled and/or lie at the interface between metastable states will be prioritized as starting simulation conditions. Figure 1 illustrates this selection criterion at play on a chaotic deterministic model, termed the Lorenz system.[63] Here, a two-state VAMPNet was trained on a trajectory with initial conditions $\boldsymbol{x}_0 = (8,7,15)^{\mathrm{T}}$ and default deeptime[50] parameters for $\{\sigma, \beta, \rho, h\}$. When projecting the output of this VAMPNet on a different trajectory obtained with $\boldsymbol{x}_0 = (7, 8, 14)^{\mathrm{T}}$, it is clearly observed that the data points that maximize the entropy (black dots) correspond to transitions between lobes (Figure 1B). In the rest of the paper, we refer to this method as MaxEnt VAMPNet or MaxEnt for brevity.

3. RESULTS AND DISCUSSION

3.1. Uncertainty-Based Selection Criteria Achieve Superior Exploration Performance. We begin by comparing the techniques described in section 2.2 using a pentapeptide of the sequence WLALL.[52] This model is small enough to quickly prototype and test different methods, but it also contains a nontrivial number of degrees of freedom and slow variables. For details about the simulations, refer to the Supporting Information methods.

The input features used to fit the kinetic models were all ϕ and ψ dihedral angles (eight features in total; ϕ_1 and ψ_5 are undefined). The models were used to project the conformations in 2D space. For the VAMPNets, a MLP[37] was employed with lobe duplication.[40] The dimensions of each layer were [8, 15, 10, 10, 5, 2] with a rectified linear unit (ReLu) as the activation function. These were also the dimensions of the TVAE's encoder, while the decoder was an MLP with dimensions [2, 5, 10, 10, 15, 8]. In all cases, the lagtime was set to 20 ps, and the batch size was 1024. We do not split the collected data into training and validation sets because our goal is to maximize the exploration rather than to validate the quality of the kinetic model. Keeping trajectories out of the analysis would preclude selecting starting structures from them.

All simulations were started from the same two metastable structures obtained from a previous study.[52] The clustering method utilized was regular space clustering (implemented in deeptime)[50] with identical parameters in all cases (max distance = 0.001, max centers = 10^4). For MA REAP, two agents with "equal" stakes and the "collaborative" regime[17] were used. As for other MA REAP parameters, CV weights were initialized as $\{\mathbf{w}_0^a\}_{a=1}^N = [0.5, 0.5]$, $\delta = 0.05$, and 50 LC candidates were selected per round.[60] Each round consisted of 5 trajectories of 2 ns each and 100 training epochs of the DNN-based kinetic models. We ran all methods for 60 rounds with 20 replicates each (total simulated time of 96 μs).

Figure 2 shows the results of the comparison in terms of the volume of dihedral space explored by each technique against the LC baseline. Dihedral space refers to a vector space where each dimension corresponds to a dihedral angle in the molecule (see Figure S1). Figure 2A shows the results for the methods employing a combination of LC adaptive sampling and a kinetic model, while Figure 2B shows the

https://doi.org/10.1021/acs.jctc.3c00040
J. Chem. Theory Comput. XXXX, XXX, XXX−XXX

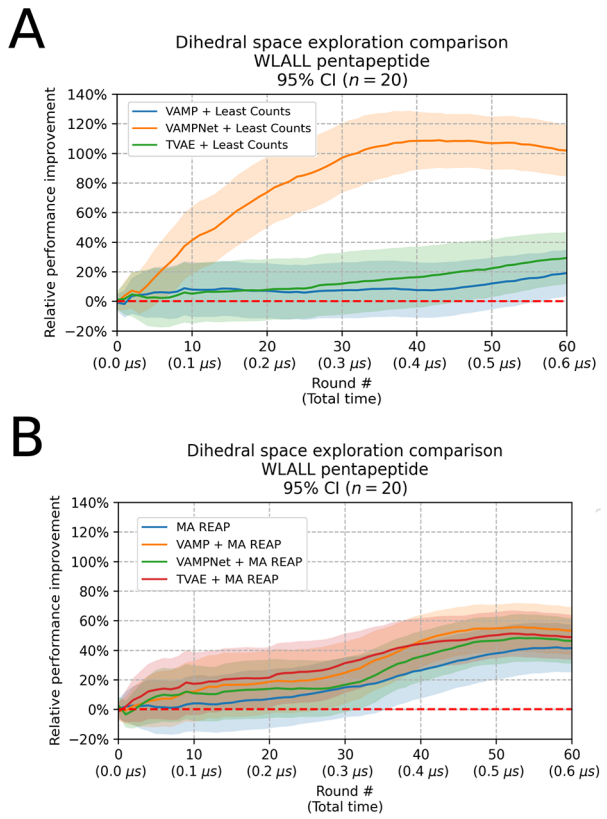

Figure 2. Relative increase in dihedral space volume explored on WLALL pentapeptide across the techniques. The same baseline, LC adaptive sampling with no kinetic model, was used in both plots (dashed line). Curves show mean for 20 replicates with a 95% CI. (A) Comparison with {VAMP, VAMPNet, TVAE} + LC. (B) Comparison with MA REAP and {VAMP, VAMPNet, TVAE} + MA REAP.

same results for the techniques involving MA REAP. Figure 2A shows that combining LC adaptive sampling with a VAMPNet produced a considerable advantage against the LC baseline (100% increase in explored volume after 600 ns). On the other hand, TVAE + LC only yielded an advantage of approximately 25%, but for $t < 600$ ns, the difference is smaller and not statistically significant. VAMP + LC did not yield a statistically significant advantage for the length of the simulations tested. The results from Figure 2B show that MA REAP increased the explored volume by approximately 40% after 60 rounds, but in this case, the use of the kinetic models only produced marginal gains. The difference in performance between MA REAP and the combination of {VAMP, VAMPNet, TVAE} + MA REAP was not statistically significant.

Figure 3 provides a visual depiction of dihedral space exploration by the baseline (LC) and the best method (VAMPNet + LC). The figure shows the Ramachandran plots for the three central amino acids in the WLALL peptide for the first three replicates (for all replicates, see Figures S2–S5). These plots show that the states with $\phi_2 > 0$ were not thoroughly explored by LC, whereas most replicates for VAMPNet + LC discovered this portion of the landscape.

The first point of interest raised by these results is the success of VAMPNet + LC at accelerating exploration, even when compared to VAMPNet + MA REAP, which uses the same kinetic model and a more sophisticated adaptive sampling regime. This result can be explained by the fact that the reward function in MA REAP (eq 3) relies on a distance metric between the states and the distribution mean. Since the kinetic model is fit with a data set that incorporates new trajectories after each round, the mapping from feature space to latent space changes, distorting distances, and, consequently, the deviations of the states. This is likely to result in an inefficient estimation of the weights that MA REAP utilizes to prioritize a given direction in exploration. Thus, we observe poor performance gains from combining MA REAP and a kinetic model. Another important comparison to make is that between VAMPNet + LC and {VAMP, TVAE} + LC. In this case, the same adaptive sampling regime is used but the kinetic model changes. The poor performance of VAMP + LC against VAMPNet + LC arises from the fact that a linear method is inefficient at discriminating between kinetically distinct states because the boundaries are not linear in dihedral space. On the other hand, TVAE is also based on a DNN, and

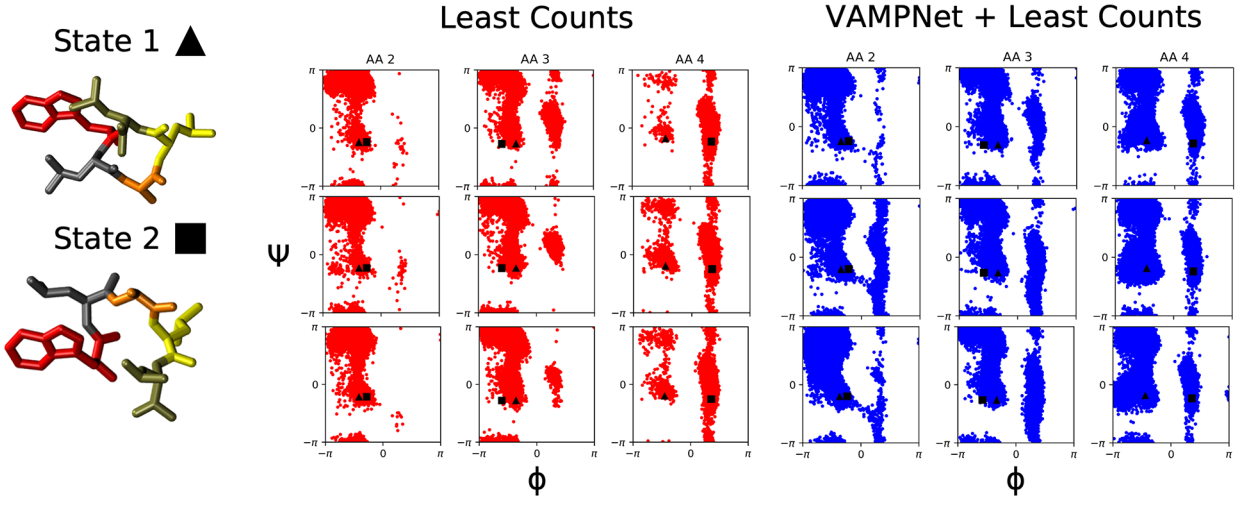

Figure 3. Ramachandran plots for central amino acids in the WLALL peptide for the baseline method (LC) and most successful method (VAMPNet + LC). Each row corresponds to a different replicate, each column to a different amino acid. (Left) Initial states employed in all simulations. These conformations were projected on the plots. (Center) Ramachandran plots for LC. (Right) Ramachandran plots for VAMPNet + LC.

https://doi.org/10.1021/acs.jctc.3c00040
J. Chem. Theory Comput. XXXX, XXX, XXX−XXX

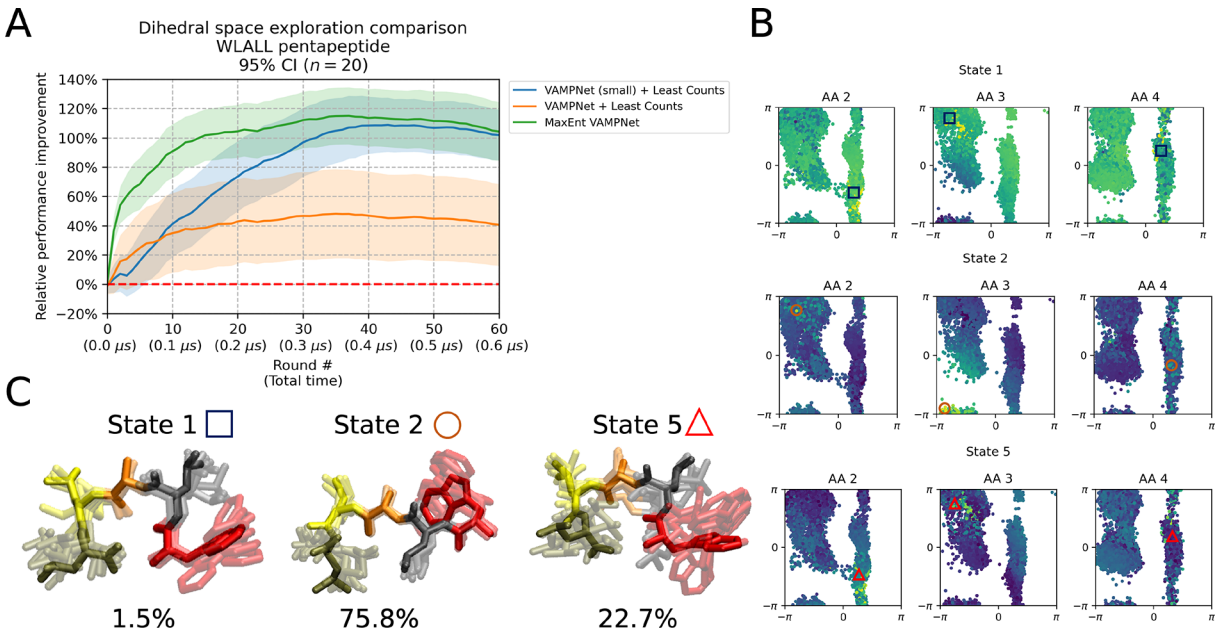

Figure 4. Results for comparison involving MaxEnt VAMPNet. (A) Relative increase in dihedral space volume explored on the WLALL peptide across techniques. LC adaptive sampling with no kinetic model (dashed line), was used as baseline. Curves show mean for 20 replicates with a 95% CI. (B) Projection of the three VAMPNet states with non-empty populations on the Ramachandran plots of L2-A3-L4 from the first replicate of MaxEnt. (C) Conformations that maximize the probability for the output states 1, 2, and 5 from (B). Percentage populations are shown below each state.

the encoder can learn a latent space that separates the metastable states. However, training a variational autoencoder is more demanding than training a MLP, as the TVAE must learn the probability distribution over the latent space, and a decoder must be simultaneously fit. Although it remains interesting to utilize models such as TVAEs (which allow for generative inference) in future applications, in this study we limit ourselves to observe that they do not accelerate adaptive sampling at a rate similar to that of simpler MLP-based models (VAMPNets).

Overall, in this section, we showed that VAMPNet + LC achieved an advantage of ∼100% against the LC baseline and ∼60% against MA REAP methods in the pentapeptide model. This observation motivated the steps taken in the following section.

3.2. MaxEnt Achieves Faster Discovery of the Conformational Landscape. Inspired by the results from the previous section, we further investigated the origin of the large advantage displayed by VAMPNet + LC. In general, LC is better than continuous MD simulations, because it prioritizes the sampling of poorly characterized states. We hypothesized that a determining factor in the success of VAMPNet + LC is the selection of data points that lead to "informative" trajectories for the VAMPNet. In other words, LC selected structures that resulted in better training examples for the DNN model, allowing a productive separation of states in the latent space and thus encouraged the discovery of new regions of the conformational landscape in future iterations. If this is the case, then another selection regime that queries data points to maximize learning should result in advantageous exploration, even if that regime is not related to a known adaptive sampling technique. For this reason, we decided to utilize entropy-based sampling, which is a common choice in the active learning community (see Methods) and termed the new method MaxEnt VAMPNet. In this method, the output of the VAMPNet is not interpreted as coordinates in latent space but rather as membership probabilities in the output states. For this reason, we used a larger output layer (eight states) and included a softmax layer as the final operation. The number of parameters in the hidden layers were also increased; the new dimensions were [8, 16, 32, 64, 128, 256, 128, 64, 32, 16, 8]. New runs with VAMPNet + LC were performed with identical layer sizes to observe the effect of increasing the number of parameters. The number of training epochs per round was kept at 100, but the batch size was increased to 2048. Other details were identical to those in the previous section. The length of trajectories, number of rounds, and number of replicates were also kept identical for a total simulated time of 36 μs.

Figure 4 shows the results from this trial. The VAMPNet + LC result from the previous section is also plotted in Figure 4A for clarity. This plot shows that MaxEnt reached the same level of performance improvement as VAMPNet + LC (with the smaller DNN from the previous section). However, the entropy-based method reached this level of advantage after only ∼150 ns instead of ∼300 ns for VAMPNet + LC. It is important to observe that using a larger VAMPNet with more output dimensions harms the performance of VAMPNet + LC. This is likely due to the fact that the quality of clustering degrades when using eight output dimensions instead of two. This highlights an advantage of MaxEnt, as this technique does not rely on clustering and state assignment is handled directly by the VAMPNet. For a projection of the data from all replicates of MaxEnt on Ramachandran plots, see Figures S6 and S7.

Although we do not expect MaxEnt to produce a fully validated kinetic model, we inspected the output of the VAMPNet obtained by this technique. Figure 4B shows the projection on Ramachandran plots of the only three states with nonempty memberships obtained from the first replicate of MaxEnt. In general, we observe gradients that indicate that the

https://doi.org/10.1021/acs.jctc.3c00040
J. Chem. Theory Comput. XXXX, XXX, XXX−XXX

VAMPNet has learned a useful separation of states in dihedral space. However, state 5 shows very diverse conformations, unlike states 1 and 2 (Figure 4C), showing that the model could lump unrelated conformations into the same state.

While adaptive sampling techniques are traditionally used to obtain converged thermodynamic and kinetic properties with shorter trajectories, many previous studies, including recent applications[20] of these techniques, split the sampling into two stages: exploration and extensive simulations. In the exploration phase, the goal is to cover as much of the conformational landscape as possible to obtain informative seeds (i.e., states that are representative of the conformational ensemble) for the following phase, where the researcher will run longer simulations to obtain better estimates of thermodynamic and kinetic properties. The advantage of this two-stage approach (as opposed to simply running long simulations initially) is that using shorter trajectories accelerates the discovery of the conformational landscape, which reduces the time needed by the long trajectories to encounter the system's states for the first time. Our algorithms are intended to tackle the first phase of this two-stage approach.

Nonetheless, we have fitted Markov State Models (MSMs)[24] on the pentapeptide data sets for the three most relevant methods: the Least Counts baseline and the two most competitive methods, VAMPNet (small network) + LC and MaxEnt VAMPNet. To fit an MSM, we use regular space clustering (as implemented in deeptime[50]) with 3000 max clusters and 1.4 minimum distance. We use PCCA[64] to obtain a three-macrostate model. The lagtime used was 32 timesteps. The state populations are shown in Figure S8. The implied time scales (ITS) are shown in Figure S9. The Chapman−Kolmogorov (CK) test results are presented in Figures S10−S12. The tests show that the MSMs obtained with VAMPNet + LC and MaxEnt show converged ITS and are Markovian, while the MSM fitted on the LC data set does not show these properties.

In summary, in this section we showed that MaxEnt can achieve the same advantage as VAMPNet + LC in a shorter amount of time, suggesting that the former option is a more favorable choice of the adaptive sampling regime. In the following section, we compare these two techniques in a more realistic model to assess whether the trends observed in the pentapeptide model translate to a larger protein.

3.3. MaxEnt Shows an Advantage in a Realistic System. The villin headpiece subdomain (PDB ID: 1YRF)[65] is a 35 amino acid, fast-folding protein that represents a more realistic system for MD simulations. The input features used were all pairwise C_α distances (separated by at least two residues). Therefore, we obtained 528 features. Since the number of features is too large to produce a reasonable clustering for LC without applying dimensionality reduction techniques, we drop this baseline and instead use VAMPNet + LC as the standard to assess the performance of MaxEnt. According to the results from the previous sections, this new baseline is significantly more demanding than vanilla LC. In all cases, the dimensions of the VAMPNets were [528, 512, 256, 128, 64, 32, 16, 8]. Batch size was set to 1024 and lobe duplication was employed. Lagtime used was 100 ps. Each round consisted of 10 trajectories of 10 ns each and 100 training epochs for the VAMPNet. We performed 10 replicates per method with 10 rounds per replicate (total simulated time of 20 μs). Other details were identical to those in previous sections. For details about the MD simulations, refer to the Supporting Information methods.

Since it is impractical to compute the explored volume in a 528-dimensional space, we pool all the data from both methods and fit a VAMP model to project the trajectories onto a common 8-dimensional tIC space. We then computed the explored volume in this space. Figure 5 shows the

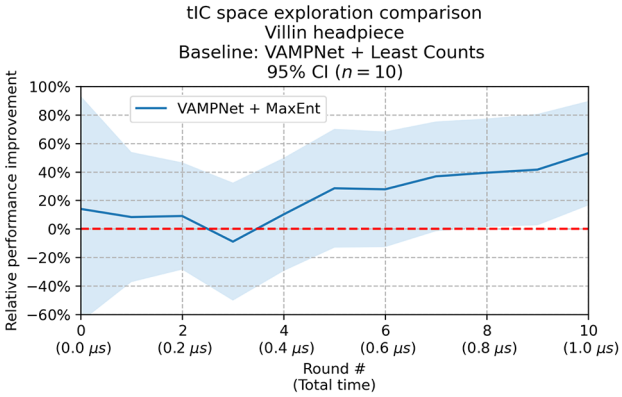

Figure 5. Relative increase in tIC space volume explored for MaxEnt simulations of the villin headpiece subdomain. VAMPNet + LC (dashed line) was used as baseline. The curve shows the mean for 10 replicates with a 95% CI.

comparison for VAMPNet + LC vs MaxEnt. We can observe that there are no statistically significant differences between the two methods until t = 700 ns. After 1 μs, MaxEnt shows an average exploration advantage of ∼50% with a 95% confidence interval of approximately [20%, 90%]. The volume explored by individual replicates is plotted in Figure S13 to easily observe the distribution for each method.

Figure 6A shows the tIC1−tIC2 landscapes for the first replicate of each method and for a single continuous trajectory of the same total length. The landscapes for all replicates are available in Figures S14−S17. While 1 μs simulations are insufficient to observe unfolding at T = 300 K, we can observe differences in the conformational ensemble explored by MaxEnt since it discovers an area of the landscape that remains uncharted by the continuous trajectory and VAMPNet + LC.

Figure 6B shows a representative set of conformations discovered by each technique. State 1 represents the native folded structure; state 2 is a "closed" conformation where the C-terminus interacts with F51 and G52, state 3 is a conformation where the N-terminal α-helix bends perpendicularly to the plane spanned by the two other α-helices, and state 4 (often observed by MaxEnt but not by VAMPNet + LC) is an intermediate state between 2 and 3. MaxEnt shows improved performance compared to VAMPNet + LC due to its ability to choose starting conformations that are more likely to result in the sampling of kinetically distinct states. This is a consequence of the entropy score, which specifically targets conformations that cannot be confidently assigned to a metastable state. In the villin headpiece simulations, this can be observed as MaxEnt samples state 4 (Figure 6B) with a higher chance than that of VAMPNet + LC, resulting in a higher explored volume.

In summary, MaxEnt showed a statistically significant advantage in exploration against the challenging VAMPNet + LC baseline in a realistic system, indicating that entropy-based

https://doi.org/10.1021/acs.jctc.3c00040
J. Chem. Theory Comput. XXXX, XXX, XXX−XXX

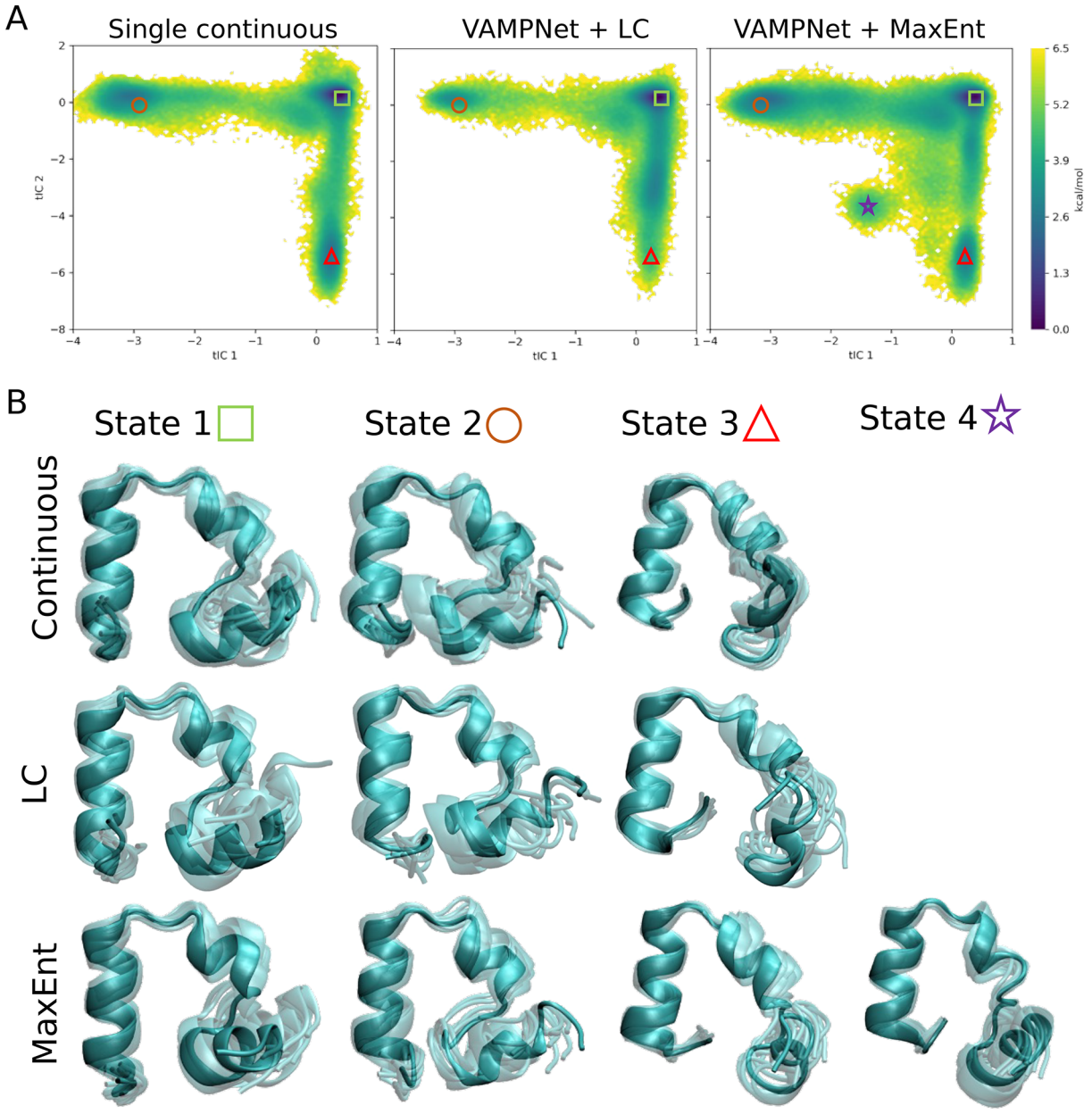

Figure 6. (A) tIC1−tIC2 landscapes for the villin headpiece corresponding to the first replicate of each method. (B) Representative conformations of different states discovered by each technique.

sampling is likely to be a better choice between these two techniques. Due to the long time scale of villin unfolding,[10] neither method reached a denatured conformation, but this was expected for the simulation conditions.

4. CONCLUSIONS

In this study, we propose new techniques involving active learning of DNN-based kinetic models to accelerate exploration in adaptive sampling MD simulations. Our results show that entropy-based sampling of a VAMPNet achieves the fastest exploration of the conformational landscape in both simulated systems. Besides showing better exploration behavior, VAMPNet grants MaxEnt the convenience of skipping the clustering step altogether. This eliminates design decisions, because clustering parameters must be set. Using a suboptimal set of clustering parameters in adaptive sampling can frustrate the rate of exploration or obfuscate subsequent data analysis.

However, MaxEnt also suffers from limitations. Training a VAMPNet in each iteration of adaptive sampling can be time-consuming and computationally intensive. Nonetheless, this task is expected to represent a small fraction of the computational expense in adaptive sampling because MD simulations of large systems remain slow in comparison. Another challenge in the use of VAMPNets for adaptive sampling is their validation. Arguably, a researcher has a few options to validate the model at each sampling iteration: (1) set aside some trajectories to use as an uncorrelated validation set, (2) exclude some random $\{\boldsymbol{x}_t, \boldsymbol{x}_{t+\tau}\}$ pairs to use as a (correlated) validation set, or (3) use some k-fold cross validation approach. All options have advantages and downsides. For (1), setting aside entire trajectories can harm the exploration rate since the validation conformations cannot be

https://doi.org/10.1021/acs.jctc.3c00040
J. Chem. Theory Comput. XXXX, XXX, XXX−XXX

selected to restart simulations. However, this method ensures that the validation set is uncorrelated with the training set; therefore, the validation score is more reliable. In (2), the opposite is the case. Since the validation structures are correlated to those used in training, the user can select conformations that are similar to those withheld, but the validation score may not be indicative of the true performance of the model. Finally, (3) can produce an unbiased validation score if the data are divided into uncorrelated groups. After applying *k*-fold cross validation, the model can be retrained on the entire data set to select new structures for simulation. However, this alternative is computationally expensive in comparison to (1) or (2). Validating the model may alert the researcher that the VAMPNet employed is underfitting or overfitting the data, and thus, the model must be modified before proceeding. This represents an onerous effort that is not found in other adaptive sampling algorithms. A particularly relevant validation parameter is the number of output states utilized. A simple approach to constrain this number is to compute the populations of each state with all of the available data. If there are empty states (output nodes that never achieve the maximum probability for any conformation), then these could be eliminated from the model. In our trials, we decided to test our techniques without submitting the kinetic models to validation and observe whether an exploration advantage was achieved regardless. Future work will involve studying the relationship between the validation scores and exploration performance. It must be noted that entropy-based sampling is expected to provide robustness to MaxEnt because this uncertainty metric inherently makes the least assumptions about the model's knowledge.[55]

Another limitation is the existence of corner cases regarding the entropy scores. For example, given two probability vectors $\boldsymbol{p}_1 = [0.49, 0.49, 0.02]$ and $\boldsymbol{p}_2 = [0.7, 0.15, 0.15]$, one would expect that the first one would be selected, but it actually has a lower entropy than $\boldsymbol{p}_2$. Although we did not observe this phenomenon in our data analysis, it could be mitigated by weighting the entropy score by the complement of the maximum probability, $1 - \max(\boldsymbol{p})$ (see Figure S18). Future studies will analyze the impact of this modified scoring function.

Although it is regular practice among adaptive sampling MD practitioners to use tICA[42,43] to reduce the dimensionality of the input features before applying a selection criterion to restart simulations, our tests involving similar approaches (i.e., VAMP + {LC, MA REAP}) did not yield promising results in comparison to those of VAMPNet + {LC, MaxEnt}. Nonetheless, this does not preclude that, for other systems, an advantage might be achieved by employing VAMP or tICA in combination with LC instead of applying LC on the feature space. In terms of applying MaxEnt in practice, the common workflow of adaptive sampling is not radically altered. In all adaptive sampling schemes, the data must be centralized at some point to perform the analysis step. This step can be replaced by the fitting of a VAMPNet (or an ensemble of VAMPNets for the sake of robustness) on the collected data. Once that the starting conformations are selected, the trajectories can be run in decentralized clusters as usual.

Lastly, it is important to note that, to the best of our knowledge, there is no theoretical foundation that indicates that the VAMP-2 gain function is the optimal choice to accelerate adaptive sampling through entropy-based sampling. This choice is intuitive because a VAMPNet trained to maximize this score learns to discriminate between metastable states,[40] and therefore, the conformations that maximize the Shannon entropy are more likely to be low-probability and/or poorly sampled structures. Moreover, there are several other active learning approaches besides entropy-based sampling[55] that have not been explored in this work. Future studies in this direction will explore questions of the optimal choice of the loss function and active learning regime for the purposes of adaptive sampling.

■ ASSOCIATED CONTENT

Data Availability Statement

All code necessary to reproduce the data is available on https://github.com/ShuklaGroup/MaxEntVAMPNet.

Supporting Information

The Supporting Information is available free of charge at https://pubs.acs.org/doi/10.1021/acs.jctc.3c00040.

Supporting methods and Figures S1−S18 (PDF)

■ AUTHOR INFORMATION

Corresponding Author

Diwakar Shukla − *Center for Biophysics and Quantitative Biology, University of Illinois at Urbana—Champaign, Urbana, Illinois 61801, United States; Department of Chemical and Biomolecular Engineering, Department of Bioengineering, and Department of Plant Biology, University of Illinois at Urbana—Champaign, Urbana, Illinois 61801, United States;* orcid.org/0000-0003-4079-5381; Email: diwakar@illinois.edu

Author

Diego E. Kleiman − *Center for Biophysics and Quantitative Biology, University of Illinois at Urbana—Champaign, Urbana, Illinois 61801, United States;* orcid.org/0000-0002-3833-5872

Complete contact information is available at: https://pubs.acs.org/10.1021/acs.jctc.3c00040

Notes

The authors declare no competing financial interest.

■ ACKNOWLEDGMENTS

The authors acknowledge support from the National Science Foundation Early CAREER Award (NSF MCB-1845606).

■ REFERENCES

(1) Lau, D.; Jian, W.; Yu, Z.; Hui, D. Nano-engineering of construction materials using molecular dynamics simulations: Prospects and challenges. *Compos. B. Eng.* **2018**, *143*, 282−291.

(2) Jackson, N. E. Coarse-graining organic semiconductors: the path to multiscale design. *J. Phys. Chem. B* **2021**, *125*, 485−496.

(3) Weigle, A. T.; Feng, J.; Shukla, D. Thirty years of molecular dynamics simulations on posttranslational modifications of proteins. *Phys. Chem. Chem. Phys.* **2022**, *24*, 26371.

(4) Chan, M. C.; Selvam, B.; Young, H. J.; Procko, E.; Shukla, D. The substrate import mechanism of the human serotonin transporter. *Biophys. J.* **2022**, *121*, 715−730.

(5) Feng, J.; Selvam, B.; Shukla, D. How do antiporters exchange substrates across the cell membrane? An atomic-level description of the complete exchange cycle in NarK. *Structure* **2021**, *29*, 922−933.

(6) Shukla, D.; Meng, Y.; Roux, B.; Pande, V. S. Activation pathway of Src kinase reveals intermediate states as targets for drug design. *Nat. Commun.* **2014**, *5*, 3397.

(7) Kohlhoff, K. J.; Shukla, D.; Lawrenz, M.; Bowman, G. R.; Konerding, D. E.; Belov, D.; Altman, R. B.; Pande, V. S. Cloud-based simulations on Google Exacycle reveal ligand modulation of GPCR activation pathways. *Nat. Chem.* **2014**, *6*, 15−21.
(8) Shan, Y.; Kim, E. T.; Eastwood, M. P.; Dror, R. O.; Seeliger, M. A.; Shaw, D. E. How does a drug molecule find its target binding site? *J. Am. Chem. Soc.* **2011**, *133*, 9181−9183.
(9) Chen, J.; White, A.; Nelson, D. C.; Shukla, D. Role of substrate recognition in modulating strigolactone receptor selectivity in witchweed. *J. Biol. Chem.* **2021**, *297*, 101092.
(10) Lindorff-Larsen, K.; Piana, S.; Dror, R. O.; Shaw, D. E. How fast-folding proteins fold. *Science* **2011**, *334*, 517−520.
(11) Hénin, J.; Lelièvre, T.; Shirts, M.; Valsson, O.; Delemotte, L. Enhanced Sampling Methods for Molecular Dynamics Simulations [Article v1. 0]. *Living J. Comp. Mol. Sci.* **2022**, *4*, 1583.
(12) Hamelberg, D.; Mongan, J.; McCammon, J. A. Accelerated molecular dynamics: a promising and efficient simulation method for biomolecules. *J. Chem. Phys.* **2004**, *120*, 11919−11929.
(13) Yu, T.-Q.; Lu, J.; Abrams, C. F.; Vanden-Eijnden, E. Multiscale implementation of infinite-swap replica exchange molecular dynamics. *Proc. Natl. Acad. Sci. U.S.A.* **2016**, *113*, 11744−11749.
(14) Laio, A.; Rodriguez-Fortea, A.; Gervasio, F. L.; Ceccarelli, M.; Parrinello, M. Assessing the accuracy of metadynamics. *J. Phys. Chem. B* **2005**, *109*, 6714−6721.
(15) Zimmerman, M. I.; Porter, J. R.; Sun, X.; Silva, R. R.; Bowman, G. R. Choice of adaptive sampling strategy impacts state discovery, transition probabilities, and the apparent mechanism of conformational changes. *J. Chem. Theory Comput.* **2018**, *14*, 5459−5475.
(16) Zuckerman, D. M.; Chong, L. T. Weighted ensemble simulation: review of methodology, applications, and software. *Annu. Rev. Biophys.* **2017**, *46*, 43.
(17) Kleiman, D. E.; Shukla, D. Multiagent reinforcement learning-based adaptive sampling for conformational dynamics of proteins. *J. Chem. Theory Comput.* **2022**, *18*, 5422−5434.
(18) Moffett, A. S.; Bender, K. W.; Huber, S. C.; Shukla, D. Molecular dynamics simulations reveal the conformational dynamics of Arabidopsis thaliana BRI1 and BAK1 receptor-like kinases. *J. Biol. Chem.* **2017**, *292*, 12643−12652.
(19) Zhao, C.; Shukla, D. Molecular basis of the activation and dissociation of dimeric PYL2 receptor in abscisic acid signaling. *Phys. Chem. Chem. Phys.* **2022**, *24*, 724−734.
(20) Zimmerman, M. I.; Porter, J. R.; Ward, M. D.; Singh, S.; Vithani, N.; Meller, A.; Mallimadugula, U. L.; Kuhn, C. E.; Borowsky, J. H.; Wiewiora, R. P.; et al. SARS-CoV-2 simulations go exascale to predict dramatic spike opening and cryptic pockets across the proteome. *Nat. Chem.* **2021**, *13*, 651−659.
(21) Russo, J. D.; Zhang, S.; Leung, J. M.; Bogetti, A. T.; Thompson, J. P.; DeGrave, A. J.; Torrillo, P. A.; Pratt, A.; Wong, K. F.; Xia, J.; et al. WESTPA 2.0: High-performance upgrades for weighted ensemble simulations and analysis of longer-timescale applications. *J. Chem. Theory Comput.* **2022**, *18*, 638−649.
(22) Chan, M. C.; Shukla, D. Markov state modeling of membrane transport proteins. *J. Struct. Biol.* **2021**, *213*, 107800.
(23) Aristoff, D.; Copperman, J.; Simpson, G.; Webber, R. J.; Zuckerman, D. Weighted ensemble: Recent mathematical developments. *J. Chem. Phys.* **2023**, *158*, 014108.
(24) Husic, B. E.; Pande, V. S. Markov state models: From an art to a science. *J. Am. Chem. Soc.* **2018**, *140*, 2386−2396.
(25) Blank, T. B.; Brown, S. D.; Calhoun, A. W.; Doren, D. J. Neural network models of potential energy surfaces. *J. Chem. Phys.* **1995**, *103*, 4129−4137.
(26) Smith, J. S.; Nebgen, B. T.; Zubatyuk, R.; Lubbers, N.; Devereux, C.; Barros, K.; Tretiak, S.; Isayev, O.; Roitberg, A. E. Approaching coupled cluster accuracy with a general-purpose neural network potential through transfer learning. *Nat. Commun.* **2019**, *10*, 2903.
(27) Gkeka, P.; Stoltz, G.; Barati Farimani, A.; Belkacemi, Z.; Ceriotti, M.; Chodera, J. D.; Dinner, A. R.; Ferguson, A. L.; Maillet, J.-B.; Minoux, H.; et al. Machine learning force fields and coarse-grained variables in molecular dynamics: application to materials and biological systems. *J. Chem. Theory Comput.* **2020**, *16*, 4757−4775.
(28) Wang, D.; Wang, Y.; Chang, J.; Zhang, L.; Wang, H.; E., W. Efficient sampling of high-dimensional free energy landscapes using adaptive reinforced dynamics. *Nat. Comput. Sci.* **2022**, *2*, 20−29.
(29) Guo, A. Z.; Sevgen, E.; Sidky, H.; Whitmer, J. K.; Hubbell, J. A.; de Pablo, J. J. Adaptive enhanced sampling by force-biasing using neural networks. *J. Chem. Phys.* **2018**, *148*, 134108.
(30) Sultan, M. M.; Pande, V. S. Automated design of collective variables using supervised machine learning. *J. Chem. Phys.* **2018**, *149*, 094106.
(31) McCarty, J.; Parrinello, M. A variational conformational dynamics approach to the selection of collective variables in metadynamics. *J. Chem. Phys.* **2017**, *147*, 204109.
(32) Glielmo, A.; Husic, B. E.; Rodriguez, A.; Clementi, C.; Noé, F.; Laio, A. Unsupervised Learning Methods for Molecular Simulation Data. *Chem. Rev.* **2021**, *121*, 9722−9758.
(33) Buenfil, J.; Koelle, S. J.; Meila, M. Tangent Space Least Adaptive Clustering. *ICML 2021 Workshop on Unsupervised Reinforcement Learning*, 2021; https://openreview.net/forum?id=00thAjcutwh (accessed 08-19-2021).
(34) Preto, J.; Clementi, C. Fast recovery of free energy landscapes via diffusion-map-directed molecular dynamics. *Phys. Chem. Chem. Phys.* **2014**, *16*, 19181−19191.
(35) Zimmerman, M. I.; Bowman, G. R. FAST conformational searches by balancing exploration/exploitation trade-offs. *J. Chem. Theory Comput.* **2015**, *11*, 5747−5757.
(36) Perez, A.; Herrera-Nieto, P.; Doerr, S.; De Fabritiis, G. AdaptiveBandit: A Multi-armed Bandit Framework for Adaptive Sampling in Molecular Simulations. *J. Chem. Theory Comput.* **2020**, *16*, 4685−4693.
(37) Hornik, K.; Stinchcombe, M.; White, H. Multilayer feedforward networks are universal approximators. *Neural Netw* **1989**, *2*, 359−366.
(38) Nüske, F.; Keller, B. G.; Pérez-Hernández, G.; Mey, A. S. J. S.; Noé, F. Variational Approach to Molecular Kinetics. *J. Chem. Theory Comput.* **2014**, *10*, 1739−1752.
(39) Wu, H.; Noé, F. Variational Approach for Learning Markov Processes from Time Series Data. *J. Nonlinear Sci.* **2020**, *30*, 23−66.
(40) Mardt, A.; Pasquali, L.; Wu, H.; Noé, F. VAMPnets for deep learning of molecular kinetics. *Nat. Commun.* **2018**, *9*, 5.
(41) Wehmeyer, C.; Noé, F. Time-lagged autoencoders: Deep learning of slow collective variables for molecular kinetics. *J. Chem. Phys.* **2018**, *148*, 241703.
(42) Schwantes, C. R.; Pande, V. S. Improvements in Markov state model construction reveal many non-native interactions in the folding of NTL9. *J. Chem. Theory Comput.* **2013**, *9*, 2000−2009.
(43) Pérez-Hernández, G.; Paul, F.; Giorgino, T.; De Fabritiis, G.; Noé, F. Identification of slow molecular order parameters for Markov model construction. *J. Chem. Phys.* **2013**, *139*, 015102.
(44) Wu, H.; Nüske, F.; Paul, F.; Klus, S.; Koltai, P.; Noé, F. Variational Koopman models: Slow collective variables and molecular kinetics from short off-equilibrium simulations. *J. Chem. Phys.* **2017**, *146*, 154104.
(45) Jaynes, E. T. Information Theory and Statistical Mechanics. *Phys. Rev.* **1957**, *106*, 620−630.
(46) Bottaro, S.; Bengtsen, T.; Lindorff-Larsen, K. *Methods in Molecular Biology*; Springer US, 2020; pp 219−240.
(47) Boomsma, W.; Ferkinghoff-Borg, J.; Lindorff-Larsen, K. Combining Experiments and Simulations Using the Maximum Entropy Principle. *PLoS Comput. Biol.* **2014**, *10*, No. e1003406.
(48) Amirkulova, D. B.; White, A. D. Recent advances in maximum entropy biasing techniques for molecular dynamics. *Mol. Simul.* **2019**, *45*, 1285−1294.
(49) Tian, H.; Jiang, X.; Xiao, S.; La Force, H.; Larson, E. C.; Tao, P. LAST: Latent Space-Assisted Adaptive Sampling for Protein Trajectories. *J. Chem. Inf. Model.* **2023**, *63*, 67−75.
(50) Hoffmann, M.; Scherer, M.; Hempel, T.; Mardt, A.; de Silva, B.; Husic, B. E.; Klus, S.; Wu, H.; Kutz, N.; Brunton, S. L.; et al.

https://doi.org/10.1021/acs.jctc.3c00040
J. Chem. Theory Comput. XXXX, XXX, XXX−XXX

Deeptime: a Python library for machine learning dynamical models from time series data. *Mach. Learn.: Sci. Technol.* **2022**, *3*, 015009.
(51) Bowman, G. R.; Ensign, D. L.; Pande, V. S. Enhanced Modeling via Network Theory: Adaptive Sampling of Markov State Models. *J. Chem. Theory Comput.* **2010**, *6*, 787−794.
(52) Scherer, M. K.; Trendelkamp-Schroer, B.; Paul, F.; Pérez-Hernández, G.; Hoffmann, M.; Plattner, N.; Wehmeyer, C.; Prinz, J.-H.; Noé, F. PyEMMA 2: A Software Package for Estimation, Validation, and Analysis of Markov Models. *J. Chem. Theory Comput.* **2015**, *11*, 5525−5542.
(53) Žoldák, G.; Stigler, J.; Pelz, B.; Li, H.; Rief, M. Ultrafast folding kinetics and cooperativity of villin headpiece in single-molecule force spectroscopy. *Proc. Natl. Acad. Sci. U.S.A.* **2013**, *110*, 18156−18161.
(54) Hruska, E.; Abella, J. R.; Nüske, F.; Kavraki, L. E.; Clementi, C. Quantitative comparison of adaptive sampling methods for protein dynamics. *J. Chem. Phys.* **2018**, *149*, 244119.
(55) Settles, B. *Active Learning*; Springer International Publishing, 2012.
(56) Smith, J. S.; Nebgen, B.; Lubbers, N.; Isayev, O.; Roitberg, A. E. Less is more: Sampling chemical space with active learning. *J. Chem. Phys.* **2018**, *148*, 241733.
(57) Shmilovich, K.; Mansbach, R. A.; Sidky, H.; Dunne, O. E.; Panda, S. S.; Tovar, J. D.; Ferguson, A. L. Discovery of self-assembling π-conjugated peptides by active learning-directed coarse-grained molecular simulation. *J. Phys. Chem. B* **2020**, *124*, 3873−3891.
(58) Thompson, J.; Walters, W. P.; Feng, J. A.; Pabon, N. A.; Xu, H.; Goldman, B. B.; Moustakas, D.; Schmidt, M.; York, F. Optimizing Active Learning for Free Energy Calculations. *Artif. Intell. Life Sci.* **2022**, *2*, 100050.
(59) Lindsey, R. K.; Fried, L. E.; Goldman, N.; Bastea, S. Active learning for robust, high-complexity reactive atomistic simulations. *J. Chem. Phys.* **2020**, *153*, 134117.
(60) Shamsi, Z.; Cheng, K. J.; Shukla, D. Reinforcement Learning Based Adaptive Sampling: REAPing Rewards by Exploring Protein Conformational Landscapes. *J. Phys. Chem. B* **2018**, *122*, 8386−8395.
(61) Ghorbani, M.; Prasad, S.; Klauda, J. B.; Brooks, B. R. GraphVAMPNet, using graph neural networks and variational approach to Markov processes for dynamical modeling of biomolecules. *J. Chem. Phys.* **2022**, *156*, 184103.
(62) Chen, W.; Sidky, H.; Ferguson, A. L. Nonlinear discovery of slow molecular modes using state-free reversible VAMPnets. *J. Chem. Phys.* **2019**, *150*, 214114.
(63) Lorenz, E. N. Deterministic nonperiodic flow. *J. Atmos. Sci.* **1963**, *20*, 130−141.
(64) Röblitz, S.; Weber, M. Fuzzy spectral clustering by PCCA+: application to Markov state models and data classification. *Adv. Data. Anal. Classif.* **2013**, *7*, 147−179.
(65) Chiu, T. K.; Kubelka, J.; Herbst-Irmer, R.; Eaton, W. A.; Hofrichter, J.; Davies, D. R. High-resolution x-ray crystal structures of the villin headpiece subdomain, an ultrafast folding protein. *Proc. Natl. Acad. Sci. U.S.A.* **2005**, *102*, 7517−7522.

https://doi.org/10.1021/acs.jctc.3c00040
J. Chem. Theory Comput. XXXX, XXX, XXX−XXX